Recoiling from a Kick in the Head-On Case

Dae-Il Choi,[1,2] Bernard J. Kelly,[1] William D. Boggs,[3] John G. Baker,[1] Joan Centrella,[1] and James van Meter[1]

[1] *Gravitational Astrophysics Laboratory, NASA Goddard Space Flight Center, 8800 Greenbelt Rd., Greenbelt, MD 20771, USA*

[2] *Korea Institute of Science and Technology Information, 52-11, Eoun-Dong, Yuseong-Gu, Daejeon, South Korea, 305-806*

[3] *University of Maryland, Department of Physics, College Park, MD 20742, USA*

(Dated: February 5, 2007)

Recoil "kicks" induced by gravitational radiation are expected in the inspiral and merger of black holes. Recently the numerical relativity community has begun to measure the significant kicks found when both unequal masses and spins are considered. Because understanding the cause and magnitude of each component of this kick may be complicated in inspiral simulations, we consider these effects in the context of a simple test problem. We study recoils from collisions of binaries with initially head-on trajectories, starting with the simplest case of equal masses with no spin; adding spin and varying the mass ratio, both separately and jointly. We find spin-induced recoils to be significant even in head-on configurations. Additionally, it appears that the scaling of transverse kicks with spins is consistent with post-Newtonian (PN) theory, even though the kick is generated in the nonlinear merger interaction, where PN theory should not apply. This suggests that a simple heuristic description might be effective in the estimation of spin-kicks.

PACS numbers: 04.25.Dm, 04.25.Nx, 04.30.Db, 04.70.Bw, 95.30.Sf, 97.60.Lf

I. INTRODUCTION

The coalescence of spinning black holes in a binary system is expected to occur throughout the universe, on scales ranging from stellar black holes formed as the end-products of stellar evolution to supermassive black holes that lurk at the centers of galaxies. The final merger of such systems will produce an intense burst of gravitational radiation; if this radiation is emitted asymmetrically, as in the case of unequal masses and spins, the resulting remnant black hole will experience a recoil kick. The magnitude of this kick is important in a variety of astrophysical situations, such as the cosmological evolution of supermassive black holes [1, 2, 3, 4, 5, 6, 7, 8] and the growth and retention of intermediate-mass black holes in dense stellar clusters [9, 10, 11, 12, 13, 14, 15], and it also affects the expected rates of black hole mergers for gravitational wave detectors [16]. Given the importance of recoil kicks in astrophysics, there have been numerous analytic studies of this phenomenon [17, 18, 19, 20, 21, 22, 23, 24, 25]. However, since nearly all of the recoil occurs in the regime of strong gravitational fields, numerical relativity simulations are essential to obtain accurate calculations of the kick.

Recent breakthroughs in binary black hole simulations [26, 27, 28, 29] now allow extensive studies of equal mass nonspinning black hole mergers [30, 31, 32]. Calculations of the kick resulting from mergers of nonspinning black holes with unequal masses have been carried out for mass ratios $q = m_2/m_1$ in the range $q = 1$ to $q = 0.25$ [33, 34, 35], with the maximum kick velocity estimated to be $\sim$ 175km/s for mass ratio $q \sim 0.36$ [35]. In addition, several simulations of mergers of equal mass, spinning black holes have been carried out [36, 37, 38].

Most recently, several papers have appeared that address the kicks obtained from the inspiral of spinning binaries of equal [39, 40] and unequal masses [41]. These papers find considerable kicks resulting from the addition of symmetry-breaking spins, leading to a total kick speed of $\sim$ 440km/s. Using this figure, and extrapolating to an "optimal" (from post-Newtonian considerations) orbital configuration, Campanelli *et al.* [41] suggest a maximum kick of $\sim$ 1300km/s. These substantial predictions have opened the door to exciting new possibilities in the astronomy of supermassive black holes and galactic nuclei.

Nevertheless the complexity of the binary orbital evolution may obscure details such as the direction of the final kick, and its dependence on mass ratio and spin. With this in mind, we present here a study of a simpler merger problem, which may be seen as an approximation to the final plunge to merger. We chose the head-on case as a model problem to isolate kick effects from the orbital inspiral motion. Although lacking in astrophysical likelihood, our head-on investigations have the advantage of removing directional ambiguity in the kicks produced. In particular, we can readily test the leading order PN prediction that the spin and mass-ratio contributions to the kick should be orthogonal.

In our investigation of the recoil kicks produced by the merger of spinning black holes in head-on collisions, we vary both the black hole spins and mass ratio. We find definite transverse kicks from the merger of equal-mass holes with spin. Furthermore, the total kick momentum imparted appears to scale roughly with the sum of the black hole spin parameter $a_1 + a_2$. For the cases investigated, these kicks yield transverse kick velocities in the range $\sim 15 - 30$km/s. We have also seen longitudinal (along the line of motion of the holes) kicks, due to a non-unity mass ratio. These kicks are much more mod-

est in magnitude, with velocities of $\sim 2-5$km/s for the mild mass ratio chosen.

This work is carried out using the moving puncture method [27, 28, 42, 43, 44, 45]. We describe our initial data in Sec. II and our numerical methodology in Sec. III. Code calibration and testing is presented in Sec. IV. We present our results in Sec. V and conclude with a discussion in Sec. VI.

II. INITIAL DATA

We set up initial data for binary black holes represented as "punctures" [46]. The metric on the initial spacelike slice is written in the form $g_{ij} = \psi^4 \delta_{ij}$, where $i,j = 1,2,3$, with conformal factor $\psi = \psi_{\rm BL} + u$. The singular part of the conformal factor takes the form $\psi_{\rm BL} = 1 + \sum_{A=1}^{2} m_{A,p}/2|\vec{r} - \vec{r}_A|$, where the $A^{\rm th}$ black hole has mass parameter (or "puncture mass") $m_{A,p}$ and is located at coordinate position $\vec{r}_A$. The nonsingular function u is calculated by solving the Hamiltonian constraint equation using a second-order convergent elliptic solver `AMRMG` [47].

The black holes start out at rest. We use the Bowen-York [48] form of the extrinsic curvature to incorporate black hole spin:

$$K^S_{A,ij} = \frac{3}{r_A^3}\left[\epsilon_{kim} S^m_A n^k_A n_{A\,j} + \epsilon_{kjm} S^m_A n^k_A n_{A\,i}\right], \quad (1)$$

where $\vec{n}_A$ is the unit vector in the direction of increasing r_A and $\vec{S}_A$ is the spin angular momentum of the A^{th} black hole. In all cases we take $\vec{S}_A$ to be aligned with the z axis, so that $\vec{S}_A = S_A \hat{e}_z$.

In all, we consider head-on collisions for seven different initial configurations, varying the masses and spins. The initial parameters of all the simulations are listed in Table I; all length scales are given in terms of a fiducial mass M (which coincides with the ADM mass of the system for equal-mass runs). For each run, the punctures were initially placed on the y axis on the equatorial plane ($z = 0$) with the center of mass at the origin. The proper separation l between the holes, along the initial slice, is measured between the closest parts of the apparent horizons along the y axis. We note that l is not necessarily the smallest physical distance between the holes (in this spatial slice), as spin effects can twist the space-like geodesics off the coordinate axis.

We use the *horizon mass* m to define the black hole mass ratio q on the initial slice,

$$q = m_1/m_2, \quad (2)$$

where m_1 is the horizon mass of the lighter hole. The symmetric mass ratio is

$$\nu \equiv m_1\, m_2/(m_1+m_2)^2. \quad (3)$$

The horizon mass is derived from the apparent horizon's *irreducible mass* using the Christodoulou formula [49]:

$$m^2 = m_{irr}^2 + \frac{S^2}{4m_{irr}^2}, \quad (4)$$

where $m_{irr} = \sqrt{A_{AH}/16\pi}$ and A_{AH} is the area of the apparent horizon.

The spin vector $\vec{S}$ applied to each hole in the Bowen-York data prescription (1) is in fact the ADM angular momentum of that hole – the total angular momentum of the spatial slice as measured by an ADM integral at infinity if no other sources were present. Thus these parameters represent a global quantity.

The more standard definition of astrophysical black-hole spin, however, is a local one. The Kerr solution is parametrized by the black hole horizon mass m, and a spin parameter a restricted to the range of values $[0, m]$. Then, $a = |\vec{S}|/m$. We note, however, that it has proved impossible to bring Bowen-York spinning data to an a value of more than $\sim 0.927m$, significantly below the maximal Kerr value [50].

Even in the head-on case, with spin vectors orthogonal to the orbital plane, there is much freedom in the parameters describing the initial data. In particular, we have chosen to scale all distances so that the horizon mass of the lighter hole, m_1, is kept the same relative to the grid spacing (ensuring a common level of resolution of that hole's features). Within this restriction, we have also striven to maintain the same proper horizon-to-horizon separation l between the holes.

III. METHODOLOGY

These initial data sets were evolved using the moving puncture method as implemented in the `Hahndol` code [32]. We used standard BSSN evolution equations, with the addition of dissipation terms as in [51] and constraint-damping terms as in [52] in order to ensure robust stability. Our gauge conditions are 1+log lapse slicing and a hyperbolic Gamma-driver shift condition, as used in [42]; here we take $\eta = 2.0$, and the initial lapse shape chosen is $\alpha_{init} = \psi_0^{-4}$, where ψ_0 is the initial conformal factor; a

TABLE I: Simulation initial parameters in terms of a fiducial mass M. m_1 is the horizon mass of the lighter hole. q is the mass ratio defined by horizon masses. S_A^z is the non-zero component of the Bowen-York angular momentum on each hole. $a_A = |S_A|/m_A$ is the approximate Kerr spin parameter of hole A. l is the proper horizon-horizon separation of the holes. NEa$_{+-}$ and NEb$_{+-}$ are large-separation and equal-spin-parameter variants of NE$_{+-}$, as explained in the text. M_{ADM} was calculated at a finite coordinate distance from the origin ($60M$ for all but run EQ$_{+0}$).

Run	$m_{1,p}/M$	$m_{2,p}/M$	S_1^z/M^2	S_2^z/M^2	m_1/M	m_2/M	q	ν	a_1	a_2	a_1/m_1	a_2/m_2	l/M	M_{ADM}/M
EQ$_{00}$	0.5000	0.5000	0.0	0.0	0.514	0.514	1.0	0.250	0.0	0.0	0.0	0.0	12.24	1.0
NE$_{00}$	0.4909	0.7478	0.0	0.0	0.514	0.771	0.667	0.240	0.0	0.0	0.0	0.0	12.24	1.238
EQ$_{+0}$	0.3444	0.5000	0.2	0.0	0.514	0.514	1.0	0.250	0.389	0.0	0.758	0.0	12.24	1.0
EQ$_{+-}$	0.3444	0.3444	0.2	-0.2	0.514	0.514	1.0	0.250	0.389	0.389	0.758	0.758	12.4 $\pm$ 0.2	1.0
NE$_{+-}$	0.3436	0.7140	0.2	-0.2	0.516	0.773	0.668	0.240	0.388	0.259	0.752	0.335	12.6 $\pm$ 0.2	1.244
NEa$_{+-}$	0.3436	0.7140	0.2	-0.2	0.513	0.764	0.672	0.240	0.390	0.262	0.759	0.342	17.0 $\pm$ 0.2	1.250
NEb$_{+-}$	0.3436	0.5496	0.2	-0.4486	0.516	0.784	0.658	0.239	0.388	0.572	0.752	0.730	13.0 $\pm$ 0.2	1.257

steeper fall-off near the punctures than the ψ_0^{-2} used in the evolutions of [32]. Time integration was carried out with a fourth-order Runge-Kutta algorithm, and spatial derivatives with fourth-order-accurate finite differencing stencils. For the outer boundary we employed a second-order-accurate Sommerfeld condition; since the majority of our simulations here last $\sim 200M$, we locate the outer boundaries at $256M$ to ensure that there won't be any harmful effects from the boundaries. We used adaptive mesh refinement (AMR) implemented via the software package PARAMESH [53, 54], with fifth-order-accurate interpolation between refinement regions (as preservation of fourth-order accuracy in the bulk demands better than fourth-order-accurate interpolation at refinement interfaces [44, 55, 56]).

The momentum kick of the merged black hole is calculated as the aggregated time-integral of the *thrust*, dP^i/dt – a surface integral of the squared time-derivative of the radiative Weyl scalar ψ_4 times the unit radial vector [57]:

$$\frac{dP^i}{dt} = \lim_{R\to\infty}\left\{\frac{R^2}{4\pi}\oint d\Omega \frac{x^i}{R}\left|\int_{-\infty}^{t} dt\,\psi_4\right|^2\right\} \quad (5)$$

$$\Delta P^i = \int_{-\infty}^{t} dt \frac{dP^i}{dt}. \quad (6)$$

As this is quadratic in the waveform ψ_4, the kick can be expected to be weak. To perform the angular integration in (5), we use the second-order Misner algorithm described in [58, 59].

IV. CODE CALIBRATION

We have established the convergence of the `Hahndol` code in prior publications [32, 34]. To these previously published results, we have added only one qualitatively new aspect: spin on the pre-merger holes. Thus we restrict our discussion of convergence here to a study of the convergence properties of a sample spinning data set with equal masses and anti-aligned spins, EQ$_{+-}$.

Our main evolutions were performed at a maximum resolution of $M/32$ in the vicinity of the pre-merger holes. We emphasize here that, as we have maintained a smaller horizon mass of $m \sim 0.5M$ in all runs, the grid spacing realized near the smaller hole will always be close to $m/16$.

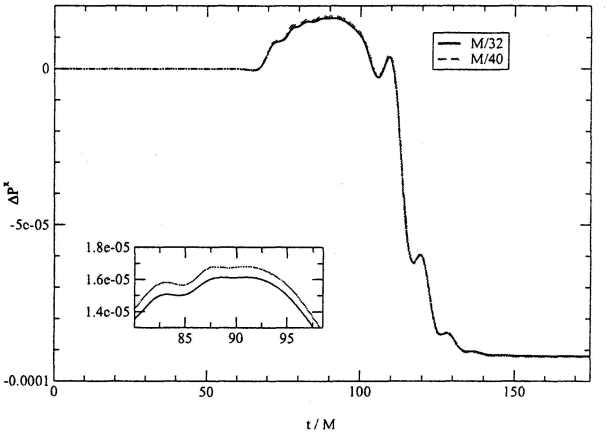

FIG. 1: Integrated transverse momentum kick ΔP^x for the EQ$_{+-}$ run at central resolutions of $M/32$ (solid/black) and $M/40$ (dashed/red).

In our simulations, the Hamiltonian constraint exhibits greater than third-order convergence, and the momentum constraint exhibits second-order convergence through most of the duration of the runs, which appears to be due to our second-order-accurate initial data solver. At late times the apparent convergence of the momentum constraint drops to a rate between first and second order; we believe this is because of a high-frequency gauge pulse propagating outward until it is insufficiently resolved at the grid resolution achieved in the outer zones of our

coarser run. However, this gauge pulse does not significantly impact the thrust computation, as evidenced by the invariance with extraction radii demonstrated in Sec. V.

In Fig. 1, we show the integrated momentum kick for our data set EQ_{+-}, at our standard resolution ($M/32$ in the most refined region), as compared with a higher ($M/40$ in the most refined region) resolution. The dominant uncertainty in our kick measurements is the accuracy of our extraction method. For the integrations performed here, the extraction method is second-order-accurate in the underlying grid resolution. Thus to estimate our error, we have assumed second-order accuracy in the integrated kick and Richardson-extrapolated our $M/32$ and $M/40$ runs. The difference between the result of this extrapolation and the $M/32$ kick is $\sim 1.2 \times 10^{-6}$; guided by this case, we take 2×10^{-6} as our error bar for all equal-mass runs.

A. Bowen-York Radiation Pulses

Bowen-York black hole initial data contains a non-negligible amount of "false radiation," even after the Hamiltonian constraint has been solved. This radiation is unphysical in the sense that it is a reflection of the unphysical approximations, such as conformal flatness, made in generating the initial data (*c.f.* [60]).

We can consider a Bowen-York black hole to be a perturbation of a Kerr hole with (to leading order) the same mass and spin. The hole relaxes to a Kerr state by radiating the perturbation through its quasinormal modes (QNMs). Assuming the spin vector is taken in the z direction, the most slowly damped QNM will be the fundamental ($l = 2, m = 2$) mode; for a hole of mass m and spin parameter $a = 0.7m$, the damping (or "e-folding") time associated with this mode is $\tau_e \approx 12m$ [61]. Judging from this, we expect the BY pulses from a pre-merger hole of mass m to have dropped two orders in magnitude after $4.6\tau_e \approx 55m$. This translates to $\sim 28M$ for our equal-mass (EQ) data sets, and $\sim 43M$ for our unequal-mass (NE) data.

This Bowen-York "pulse" is concentrated close to each hole's horizon, and much of it falls into its parent hole; however, what radiation escapes to our detection spheres will mix with the physical radiation we are generally interested in. Nevertheless, since the pulse is released immediately, and is of short duration, it should be easily identifiable in the total waveform.

To illustrate, we show in Fig. 2 the dominant ($l = 2, m = 2$) spin-2-weighted spherical harmonic mode of the "outgoing" Weyl scalar ψ_4 (extracted at $R_{ext} = 30M$), for three different equal-mass configurations: zero-spin (EQ_{00}), single-spin (EQ_{+0}) and double-spin (EQ_{+-}). Despite the differences in spins, these three waveforms agree well in the later "physical" part of the signal, with stronger differences occurring in the non-physical BY pulse. In the zero-spin case, the BY pulse is almost negligible, but it is significant for EQ_{+0} and EQ_{+-}.

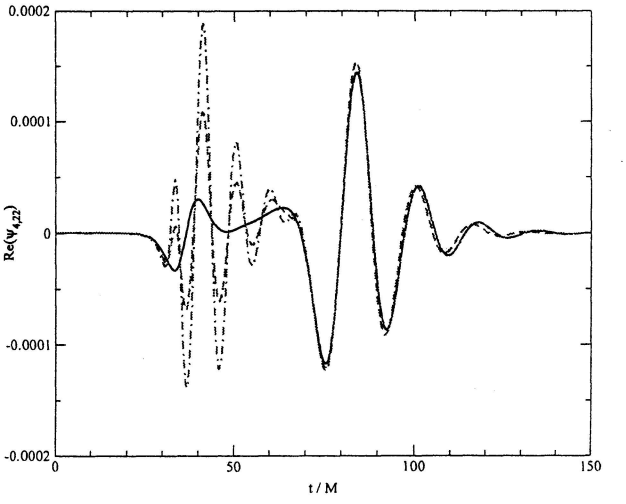

FIG. 2: Dominant ($l = 2, m = 2$) mode of the waveform ψ_4 for the three equal-mass configurations: EQ_{00} (solid/black), EQ_{+0} (dashed/red), and EQ_{+-} (dot-dashed/green) (extracted at coordinate distance $R_{ext} = 30\,M$).

This same pulse will yield a non-zero contribution to the momentum kick. Again, this should be easy to identify, as it will result in a plateau early in the run. Having identified a time at which the BY pulse and its "pseudo-kick" are finished, we remove this effect by beginning the integration of (5) from that point.

The initial separation between two black holes is chosen large enough so that the initial BY data transients are separated from the merger event. This temporal distinction means that we can choose some time t_{int} after the passage of the transient as the starting time for our numerical integration of the momentum kick.

V. RESULTS

We group our simulations into three categories. First we consider the effect of unequal masses alone, where the kick experienced should be along the line connecting the holes. We then add spins to holes of equal horizon mass, to explore the dependence of kicks on pure spin anisotropy; this configuration should yield kicks orthogonal to the line connecting the holes. Finally we consider the combination of both spin and unequal masses, to explore the interrelation of the two mechanisms generating kicks.

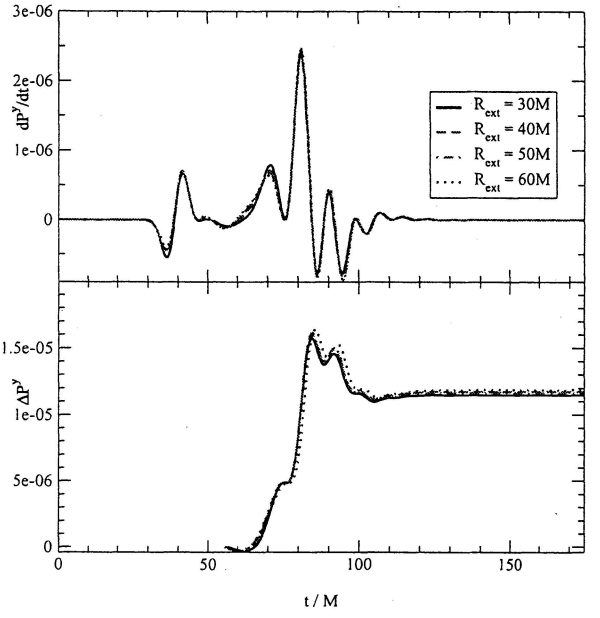

FIG. 3: Longitudinal thrust dP^y/dt (top) and kick ΔP^y (bottom) for NE_{00}, at extraction radii R_{ext} of $30M$, $40M$, $50M$ and $60M$, where the latter three have been time-shifted by $10.6M$, $21.0M$ and $30.4M$ for alignment.

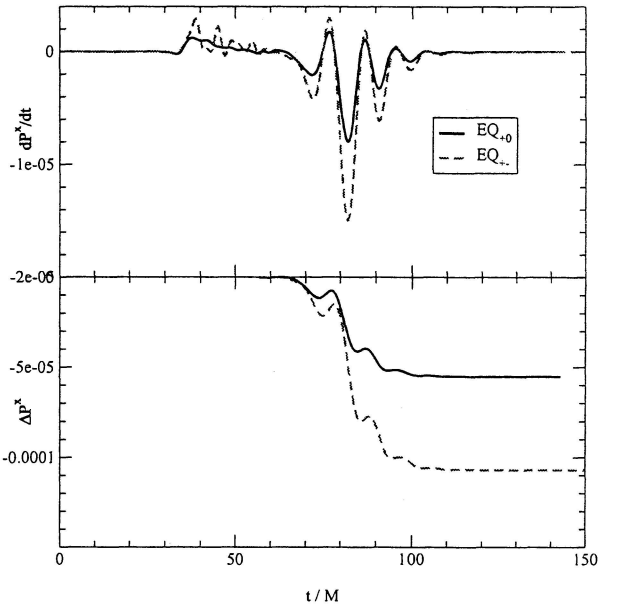

FIG. 4: Transverse thrust dP^x/dt and kick ΔP^x for the spinning, equal-mass cases EQ_{+0} (black/solid) and EQ_{+-} (red/dashed), at extraction radii R_{ext} of $30M$, where the EQ_{+-} data have been time-shifted by $1M$ to compensate for gauge differences.

A. Unequal masses without spin

The head-on collision of two holes of unequal masses has been considered several times in the past, both with close-limit analysis (CLA) [62] and with fully numerical evolutions in 2D [63]. The CLA results (performed with Misner two-sheeted data) provide a definite prediction of preferential radiation of linear momentum; the numerical results seemed to confirm this, and indicated where the CLA fails. The numerical results were for proper separations far less than ours; extrapolating their results to the larger separations we treat here indicates that a longitudinal kick of $O(10\mathrm{km/s})$ would be produced.

In Fig. 3, we plot the y-component of the thrust $d\vec{P}/dt$ from Eqn (5), and its time integral from the NE_{00} run. Note that the x and z components of $d\vec{P}/dt$ are zero: the kick is longitudinal, i.e. along the axis of collision (y axis). The final kick velocity, given in Table II, is $\sim 2.3 - 2.5\mathrm{km/s}$.

The final kick obtained from Fig. 3 is highly consistent across extraction radii, with a spread between the $R_{ext} = 30M$ and $R_{ext} = 40M$ values of $\sim 0.5\%$. We note however that the difference between $R_{ext} = 50M$ and $R_{ext} = 60M$ is larger than that between $R_{ext} = 40M$ and $R_{ext} = 50M$. This appears to be because the extraction surface at $R_{ext} = 60M$ lies in a region of less grid refinement than the three closer surfaces.

B. Equal masses with spin

We now turn to simulations of spinning black holes. We run two configurations (EQ_{+0},EQ_{+-}), as indicated in Table I. As only one particle is spinning in the former case, we should see only "spin-orbit" effects between that spin and the motion of the particle. In the latter case, with two spins, we might also see "spin-spin" effects; however PN predictions for the latter are of higher PN order than for spin-orbit [64][1].

In Fig. 4 we show the transverse kick ΔP^x observed for both equal-mass data sets. We note that both the BY pulse and the final kick for the EQ_{+-} data are roughly double those for EQ_{+0} (see Table II). This indicates that the total kick is close to a simple sum of the individual kicks. Thus any spin-spin contribution to the total kick

[1] For the EQ_{+0} run presented here, we have used slightly different choices in our numerical evolution: advection terms employed a third-order upwinding scheme, guardcell-filling was fourth-order-accurate, time stepping was performed with a second-order Crank-Nicholson method, no dissipation was used, and the initial lapse function shape was $\alpha_{init} = \psi_{BL}^{-2}$, as in the evolutions of [32]. For this data alone, the physical outer boundary was at 128 M, but the outermost extraction here was at $R_{ext} = 30M$. Aside from a $1M$ delay in the arrival of wavefronts at the extraction sphere, these minor differences have had no measurable effect on the measured kick.

is negligible in comparison to the spin-orbit term.

C. Unequal masses with spin

Having considered collisions between non-equal mass and non-spinning black holes and equal mass and spinning black holes, we combine both spin and mass ratio in a few cases, the NE_{+-}, NEa_{+-}, and NEb_{+-} runs.

We show in the upper panel of Fig. 5 the thrust for the NE_{+-} case. We note that unlike the simpler cases before, the BY pulse and physical signal are *not* obviously separated in the thrust. As a result, we may expect to have trouble determining where to begin the kick integrations.

In principle, a larger initial separation would mean more time between the BY pulse – emitted at $t = 0$ and lasting $\sim 43M$ (see discussion in Section IV A) – and the bulk of the physical radiation, which only becomes large near merger. The main physical kick will certainly be different in magnitude between the two cases, and even the BY pulse magnitude may differ, depending on the dependence of the spectrum to the initial separation of the binary. Nevertheless, we *can* expect the BY pulse duration to be the same, as the duration is determined by the leading quasinormal frequencies of each hole, and these frequencies are fully determined by the mass and spin of each hole, which is a constant between the two cases. In Fig. 5, we show dP^x/dt and ΔP^x for NE_{+-}, with a coordinate separation of $8M$, and NEa_{+-}, with a coordinate separation of $12M$.

The extra initial separation leads to a very similar physical thrust, delayed $\sim 22M$ relative to the original separation. This physical thrust begins at $\sim 114M$ for the detector at $R_{ext} = 60M$. Integrating forward from any time up to $\sim 20M$ before this will result in the same transverse kick for the NEa_{+-} case. To ensure that as much of the physical kick as possible is obtained in the smaller-separation case, we integrate the NE_{+-} thrust from $t_{int} = 114M - 22M = 92M$ at $R_{ext} = 60M$.

In Figs. 6 and 7 we present the momentum kicks in the transverse (x) and longitudinal (y) directions for the NE_{+-} data set, comparing with the kicks seen from the NE_{00} and EQ_{+-} cases before.

Taking the transverse direction first, we see from Fig. 6 that the momentum kick from NE_{+-} is significantly *smaller* than that of EQ_{+-}. The spin angular momentum S present in each case is the same, indicating that the kick is not a function of S. In contrast, the momentum kick observed from NEb_{+-} is much larger.

The physical momentum kicks from these runs are presented in Table II. We note that the ratio of transverse momentum kicks ΔP^x between the cases NE_{+-} and NEb_{+-} is roughly 2/3, consistent with the PN-derived ratio (8).

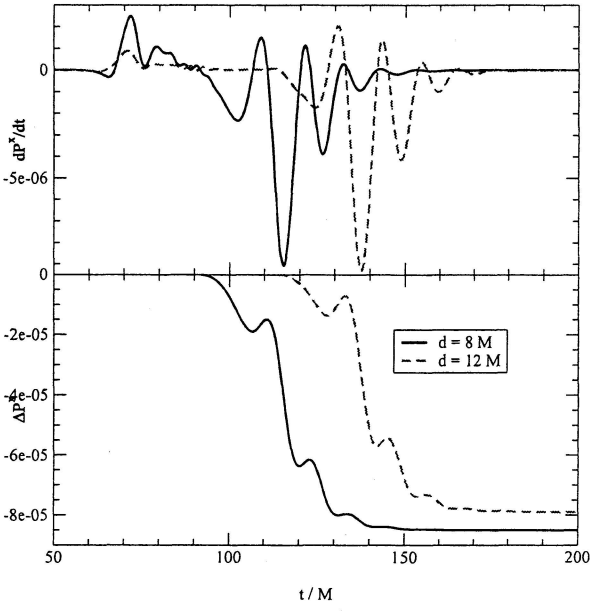

FIG. 5: Transverse thrust dP^x/dt (top) and kick ΔP^x (bottom) for unequal-mass-with-spin data, at coordinate separations $8M$ (NE_{+-}; black/solid) and $12M$ (NEa_{+-}; red/dashed). Extracted at $R_{ext} = 60M$.

In addition to finite differencing inaccuracy, for these cases we find that the high slope in the thrust for these cases yields a non-negligible error associated with the choice in integration starting point. This uncertainty is around 5.5×10^{-6} in each of ΔP^x and ΔP^y, and we conservatively assume the full uncertainty per component to be 8.0×10^{-6}, equivalent to ~ 2km/s.

With this in mind, we turn to the longitudinal direction. Here we see that the initial BY burst is comparable in magnitude to the physical later part. Using for consistency the same integration starting time as in the transverse direction, we present the longitudinal kicks in Table II. These are asterisked to emphasize our uncertainty in the kick magnitude. To this uncertainty, all longitudinal kicks are consistent with the zero-spin case, NE_{00}.

D. Summary of Results

We draw together in Table II the kicks observed in each of our simulations. We can develop some expectations for the comparative results by referencing post-Newtonian

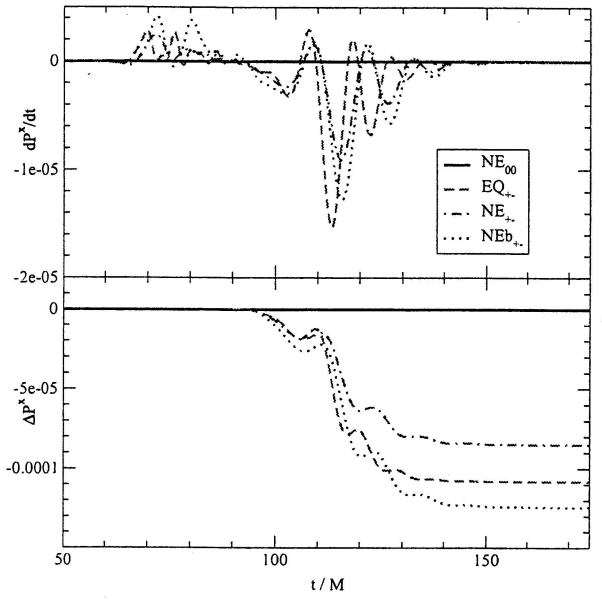

FIG. 6: Transverse thrust dP^x/dt (top) and kick ΔP^x (bottom) for NE_{00} (black), EQ_{+-} (red), and NE_{+-} (green), and NEb_{+-} (blue). Based on integrals at $R_{ext} = 60\,M$.

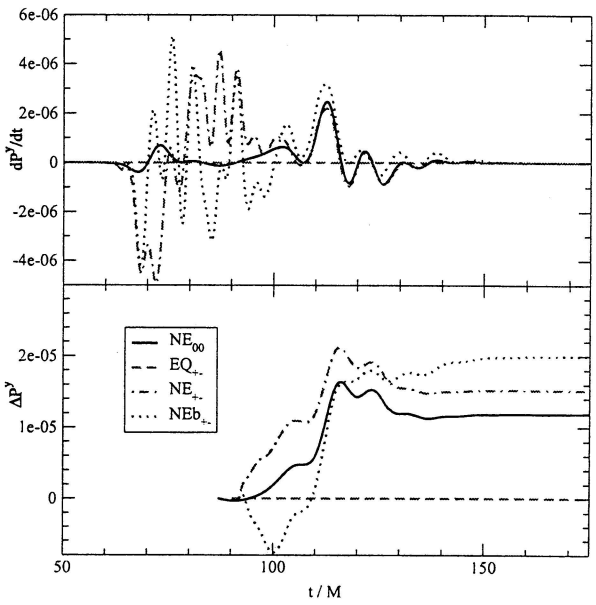

FIG. 7: Longitudinal thrust dP^y/dt (top) and kick ΔP^y (bottom) for NE_{00} (black), EQ_{+-} (red), and NE_{+-} (green), and NEb_{+-} (blue). Based on integrals at $R_{ext} = 60\,M$.

theory estimates of the radiative linear momentum loss due to unequal masses and spin-orbit coupling. For example, adapting Eqns (3.31a-b) of [64] to radial infall along the y axis, we find:

$$\dot{\vec{P}}_N = \frac{16}{105}\frac{\delta m}{m_T}\nu^2\left(\frac{m_T}{r}\right)^4 \dot{r}\left(-\dot{r}^2 + \frac{2m_T}{r}\right)\hat{e}_y, \quad (7)$$

$$\dot{\vec{P}}_{SO} = -\frac{16}{15}\frac{\nu^2\dot{r}^2}{r}\left(\frac{m_T}{r}\right)^4 (a_1 + a_2)\hat{e}_x, \quad (8)$$

where $m_T = m_1 + m_2$, $\delta m = m_1 - m_2$, and r is the spatial separation of the two particles, with $\dot{r} < 0$.

In studies of spin such as the one carried out here, whether physical effects scale with angular momentum S, the Kerr parameter $a \equiv S/m$ or the dimensionless number a/m is an open question. The Post-Newtonian result of (8) predicts a thrust (and hence kick) that scales with a for each hole. We have tried to address this uncertainty in our choice of data sets.

It is informative to compare the transverse kick results from each of our spinning data sets with each other, in light of post-Newtonian predictions. Looking at Eqn. (8), we assume that the RHS is more or less insensitive to the details of the rate of infall, the important length scale then being the total mass m_T of the binary. With this in mind, the remaining freedom lies in the spin scaling $(a_1 + a_2)/m_T$. Relative to the EQ_{+-} case, this scaling factor is $\{1/2, 2/3, 2/3, 1\}$ for cases $\{EQ_{+0}, NE_{+-}, NEa_{+-}, NEb_{+-}\}$.

In Fig. 8 we combine the post-BY-pulse part of the transverse thrust dP^x/dt of each case, with times rescaled according to the ADM mass from Table I, and translated so that the peaks coincide. We have also rescaled the thrust amplitude by the factors appropriate to the PN above Surprisingly, after this rescaling, the five thrusts fit very well, with a deviation of overall amplitude of $\sim 20\%$. This appears to indicate that PN predictions of recoil kicks have validity further into the merger regime that would be expected.

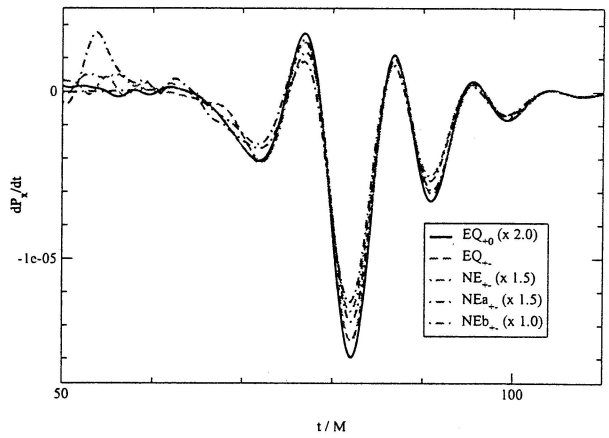

FIG. 8: Transverse thrust dP^x/dt for all spinning data sets: EQ_{+0}, EQ_{+-}, NE_{+-}, NEa_{+-}, and NEb_{+-}. Time has been rescaled by the ADM mass for each data set, and translated relative to EQ_{+-} to line up peaks. Amplitudes have been scaled relative to EQ_{+-} according to PN predictions.

TABLE II: Final integrated momentum kicks and corresponding kick velocities. In each case, we have removed "BY pulse" effects through deferring integration until after the passage of the pulse. ΔP^x and ΔP^y are accurate to $\sim 2\times10^{-6}$ for cases NE_{00}, EQ_{+0}, EQ_{+-}, corresponding to errors of $\sim$ 0.6km/s for equal-mass cases, and $\sim$ 0.5km/s in unequal-mass cases. Cases NE_{+-}, NEa_{+-}, and NEb_{+-} suffer from additional non-negligible error in the choice of integration starting point. We conservatively estimate the total error to be $\sim 8\times10^{-6}$ for these cases, translating to $\sim$ 2.0km/s in the kick velocity. Asterisks mark kick values that are dominated by this uncertainty.

Run	t_{int} (M)	ΔP^x (10^{-5})	ΔP^y (10^{-5})	v_x (km/s)	v_y (km/s)	v (km/s)
NE_{00} $30M$	51.0	0.0	1.2	0.0	2.8	2.8
$40M$	61.7	0.0	1.2	0.0	2.8	2.8
$60M$	82.9	0.0	1.2	0.0	2.9	2.9
EQ_{+0} $20M$	46.1	-5.2	0.0	-15.4	0.0	15.4
$30M$	56.6	-5.5	0.0	-16.6	0.0	16.6
EQ_{+-} $30M$	59.6	-10.7	0.0	-32.1	0.0	32.1
$40M$	70.0	-10.5	0.0	-31.6	0.0	31.6
$60M$	90.5	-10.8	0.0	-32.4	0.0	32.4
NE_{+-} $40M$	72.0	-8.5	1.4*	-20.5	3.4*	20.8
$60M$	92.0	-8.5	1.5*	-20.5	3.6*	20.8
NEa_{+-} $40M$	94.0	-7.9	1.0*	-18.9	2.4*	19.1
$60M$	114.0	-7.9	1.0*	-18.9	2.4*	19.1
NEb_{+-} $40M$	72.0	-12.3	2.0*	-29.3	4.8*	29.7
$60M$	92.0	-12.4	2.0*	-29.6	4.8*	30.0

VI. DISCUSSION

In this paper, we have addressed the roles of unequal masses and spins in producing recoil kicks in head-on collisions. We have chosen sample spins and mass ratios to explore how important spin effects are for kicks, and how the effects of spin and mass ratio are related in generating kicks. We have carried out kick extractions from data sets with mass ratios of 1 and 2/3, and with spins on one or both holes. We have observed that head-on collisions of spinning black holes can produce significant kicks. For the anti-aligned spin cases we have studied, the spin-kicks are transverse to the direction of initial separation. The magnitude of the kicks, and even the thrust curves (Fig. 8), scale with the sum of the individual black hole spin parameters $a_1 + a_2$. These kicks easily exceed the longitudinal kick produced in the case of unequal masses. To the accuracy available in our simulations, we find that the kicks due to the mass ratio and spins are indeed orthogonal and independent. Both the spin scaling and the orthogonality of spin-kicks and mass-ratio-kicks are consistent with leading-order PN predictions for these effects (7,8).

It is remarkable that the PN predictions seem to describe our results. The kick-producing radiation derived in our simulations is generated in the systems' non-linear mergers and the ringdowns where the assumptions behind the PN approximations clearly do not apply. In general terms, the PN analysis (see [64]) provides that the unequal-mass-kick is produced by a coupling of the mass-quadrupole and mass-octupole moments, while the spin-kick is produced by a coupling of the mass-quadrupole and current-quadrupole moments. At least heuristically, we can consider these moments even in the nonlinear problem. In our problem, the presence of spin does not seem to have a large effect on the mass moments, as is suggested by the spin-independence of the mass-quadrupole-dominated ($l = 2, m = 2$) waveforms, seen in Fig.2. The leading effect of putting spin on the black holes is to scale up the current-quadrupole moment. For general spins, this term scales with $(\vec{S}_1/m_1 - \vec{S}_2/m_2)$.

In the more important case of inspiraling black holes, our results suggest that the current-quadrupole effects should also provide strong kicks, scaling in a similar way with spin. Because of the scaling with S/m we would generally expect the strongest spin-kicks for nearly equal mass mergers. Our results support the use of PN expressions (as in [39, 41]) to predict the scaling of spin-kicks for black hole configurations that have not yet been studied.

Acknowledgments

This work was supported in part by NASA grant O5-BEFS-05-0044. The simulations were carried out using Project Columbia at NASA Ames Research Center and at the NASA Center for Computational Sciences at Goddard Space Flight Center. D.C. was supported in part by The Korea Research Foundation and The Korean Federation of Science and Technology Societies Grant funded by Korea Government (MOEHRD, Basic Research Promotion Fund). B.K. was supported by the Research Associateship Programs Office of the National Research Council and the NASA Postdoctoral Program at the Oak Ridge Associated Universities.

[1] D. Merritt, M. Milosavljevic, M. Favata, S. A. Hughes, and D. E. Holz, Astrophys. J. **607**, L9 (2004), astro-ph/0402057.

[2] M. Boylan-Kolchin, C.-P. Ma, and E. Quataert, Astrophys. J. **613**, L37 (2004), astro-ph/0407488.

[3] Z. Haiman, Astrophys. J. **613**, 36 (2004), astro-

ph/0404196.
[4] P. Madau and E. Quataert, Astrophys. J. **606**, L17 (2004), astro-ph/0403295.
[5] J. Yoo and J. Miralda-Escude, Astrophys. J. **614**, L25 (2004), astro-ph/0406217.
[6] M. Volonteri and R. Perna, Mon. Not. Roy. Astron. Soc. **358**, 913 (2005), astro-ph/0501345.
[7] N. I. Libeskind, S. Cole, C. S. Frenk, and J. C. Helly, Mon. Not. Roy. Astron. Soc. **368**, 1381 (2006), astro-ph/0512073.
[8] M. Micic, T. Abel, and S. Sigurdsson (2006), astro-ph/0609443.
[9] M. C. Miller and D. P. Hamilton, Mon. Not. Roy. Astron. Soc. **330**, 232 (2002), astro-ph/0106188.
[10] M. C. Miller and D. P. Hamilton, Astrophys. J. **576**, 894 (2002).
[11] H. Mouri and Y. Taniguchi, Astrophys. J. **580**, 844 (2002), astro-ph/0208053.
[12] M. C. Miller and E. J. M. Colbert, Int. J. Mod. Phys. **D13**, 1 (2004), astro-ph/0308402.
[13] K. Gultekin, M. C. Miller, and D. P. Hamilton, Astrophys. J. **616**, 221 (2004), astro-ph/0402532.
[14] K. Gultekin, M. Coleman Miller, and D. P. Hamilton, Astrophys. J. **640**, 156 (2006), astro-ph/0509885.
[15] R. M. O'Leary, F. A. Rasio, J. M. Fregeau, N. Ivanova, and R. O'Shaughnessy, Astrophys. J. **637**, 937 (2006), astro-ph/0508224.
[16] A. Sesana, F. Haardt, P. Madau, and M. Volonteri, Astrophys. J. **623**, 23 (2005), astro-ph/0409255.
[17] A. Peres, Phys. Rev. **128**, 2471 (1962).
[18] J. D. Bekenstein, Phys. Rev. D **183**, 657 (1973).
[19] M. J. Fitchett, Mon. Not. R. Astron. Soc. **203**, 1049 (1983).
[20] M. J. Fitchett and S. Detweiler, Mon. Not. R. Astron. Soc. **211**, 933 (1984).
[21] I. Redmount and M. J. Rees, Commun. Astrophys. **14**, 165 (1989).
[22] A. G. Wiseman, Phys. Rev. D **46**, 1517 (1992).
[23] M. Favata, S. A. Hughes, and D. E. Holz, Astrophys. J. **607**, L5 (2004), astro-ph/0402056.
[24] L. Blanchet, M. S. S. Qusailah, and C. M. Will, Astrophys. J. **635**, 508 (2005), astro-ph/0507692.
[25] T. Damour and A. Gopakumar, Phys. Rev. D **73**, 124006 (2006), gr-qc/0602117.
[26] F. Pretorius, Phys. Rev. Lett. **95**, 121101 (2005), gr-qc/0507014.
[27] M. Campanelli, C. O. Lousto, P. Marronetti, and Y. Zlochower, Phys. Rev. Lett. **96**, 111101 (2006), gr-qc/0511048.
[28] J. G. Baker, J. Centrella, D.-I. Choi, M. Koppitz, and J. van Meter, Phys. Rev. Lett. **96**, 111102 (2006), gr-qc/0511103.
[29] M. Campanelli, C. O. Lousto, and Y. Zlochower, Phys. Rev. D **73**, 061501 (2006), gr-qc/0601091.
[30] J. G. Baker, J. Centrella, D.-I. Choi, M. Koppitz, and J. van Meter, Phys. Rev. D **73**, 104002 (2006), gr-qc/0602026.
[31] A. Buonanno, G. B. Cook, and F. Pretorius, unpublished (2006), gr-qc/0610122.
[32] J. G. Baker, S. T. McWilliams, J. R. van Meter, J. Centrella, D.-I. Choi, B. J. Kelly, and M. Koppitz (2006).
[33] F. Herrmann, D. Shoemaker, and P. Laguna (2006), gr-qc/0601026.
[34] J. G. Baker, J. Centrella, D.-I. Choi, M. Koppitz, J. van Meter, and M. C. Miller, Astrophys. J. Lett. **653**, L93 (2006), astro-ph/0603204.
[35] J. A. Gonzalez, U. Sperhake, B. Brügmann, M. Hannam, and S. Husa, unpublished (2006), gr-qc/0610154.
[36] M. Campanelli, C. O. Lousto, and Y. Zlochower, Phys. Rev. D **74**, 041501 (2006), gr-qc/0604012.
[37] M. Campanelli, C. O. Lousto, and Y. Zlochower, Phys. Rev. D **74**, 084023 (2006), astro-ph/0608275.
[38] M. Campanelli, C. O. Lousto, Y. Zlochower, B. Krishnan, and D. Merritt (2006), gr-qc/0612076.
[39] F. Herrmann, I. Hinder, D. Shoemaker, P. Laguna, and R. A. Matzner (2007), gr-qc/0701143.
[40] M. Koppitz, D. Pollney, C. Reisswig, L. Rezzolla, J. thornburg, P. Diener, and E. Schnetter (2007), gr-qc/0701163.
[41] M. Campanelli, C. O. Lousto, Y. Zlochower, and D. Merritt (2007), gr-qc/0701164.
[42] J. R. van Meter, J. G. Baker, M. Koppitz, and D.-I. Choi, Phys. Rev. D **73**, 124011 (2006), gr-qc/0605030.
[43] M. Hannam, S. Husa, D. Pollney, B. Brügmann, and N. Ó Murchadha (2006), gr-qc/0606099.
[44] B. Brügmann, J. A. Gonzalez, M. Hannam, S. Husa, U. Sperhake, and W. Tichy (2006), gr-qc/0610128.
[45] U. Sperhake (2006), gr-qc/0606079.
[46] S. Brandt and B. Brügmann, Phys. Rev. Lett. **78**, 3606 (1997), gr-qc/9703066.
[47] J. D. Brown and L. L. Lowe, J. Comput. Phys. **209**, 582 (2005), gr-qc/0411112.
[48] J. Bowen and J. W. York, Phys. Rev. D **21**, 2047 (1980).
[49] D. Christodoulou, Phys. Rev. Lett. **25**, 1596 (1970).
[50] S. Dain, C. O. Lousto, and R. Takahashi, Phys. Rev. D **65**, 104038 (2002), gr-qc/0201062.
[51] P. Hübner, Class. Quantum Grav. **16**, 2823 (1999).
[52] M. D. Duez, S. L. Shapiro, and H.-J. Yo, Phys. Rev. D **69**, 104016 (2004), gr-qc/0401076.
[53] P. MacNeice, K. Olson, C. Mobarry, R. de Fainchtein, and C. Packer, Computer Physics Comm. **126**, 330 (2000).
[54] `http://ct.gsfc.nasa.gov/paramesh/Users_manual/amr.html`.
[55] B. Imbiriba et al., Phys. Rev. D **70**, 124025 (2004), gr-qc/0403048.
[56] L. Lehner, S. L. Liebling, and O. Reula, Class. Quantum Grav. **23**, S421 (2006), gr-qc/0510111.
[57] E. T. Newman and K. P. Tod, in *General Relativity and Gravitation: One hundred years after the birth of Albert Einstein, vol. 2*, edited by A. Held (Plenum Press, NY, 1981), pp. 1–36.
[58] C. W. Misner, Class. Quantum Grav. **21**, S243 (2004), gr-qc/9910044.
[59] D. R. Fiske, J. G. Baker, J. R. van Meter, D.-I. Choi, and J. M. Centrella, Phys. Rev. D **71**, 104036 (2005), gr-qc/0503100.
[60] M. Hannam, S. Husa, B. Brügmann, J. A. Gonzalez, and U. Sperhake (2006), gr-qc/0612001.
[61] E. Berti, V. Cardoso, and C. M. Will, Phys. Rev. D **73**, 064030 (2006), gr-qc/0512160.
[62] Z. Andrade and R. H. Price, Phys. Rev. D **56**, 6336 (1997), gr-qc/9611022.
[63] P. Anninos and S. Brandt, Phys. Rev. Lett. **81**, 508

(1998), gr-qc/9806031.
[64] L. Kidder, Phys. Rev. D **52**, 821 (1995), gr-qc/9506022.